Title
VACANCY AGGREGATES IN QUENCHED COPPER SINGLE CRYSTALS

Authors
Bell, W.
Maher, D.M.
Thomas, G.

Publication Date
1964-06-01

UCRL-11480

University of California

Ernest O. Lawrence Radiation Laboratory

VACANCY AGGREGATES IN QUENCHED COPPER SINGLE CRYSTALS

Berkeley, California

DISCLAIMER

To appear in the Proceedings of
the International Conference on
Lattice Defects in Quenched
Metals, ANL, June 15-17, 1964

UCRL-11480

UNIVERSITY OF CALIFORNIA

Lawrence Radiation Laboratory
Berkeley, California

AEC Contract No. W-7405-eng-48

VACANCY AGGREGATES IN QUENCHED COPPER SINGLE CRYSTALS

W. Bell, D. M. Maher and G. Thomas

June, 1964

VACANCY AGGREGATES IN QUENCHED COPPER SINGLE CRYSTALS*

W. Bell, D. M. Maher and G. Thomas

Inorganic Materials Research Division, Lawrence Radiation Laboratory
and Department of Mineral Technology, University of California
Berkeley, California

Abstract

Copper single crystals of 99.999+ purity have been gas quenched from vacuum and aged under controlled conditions. In all cases planar, vacancy aggregates have been identified by dark field electron microscopy techniques. Both perfect and imperfect prismatic loops have been observed, but the former appear to be more numerous. The maximum size of imperfect loops does not exceed 125Å, whereas, perfect loops range in size from 100 to 200 Å. The results suggest that the perfect loop forms from the imperfect loop at some critical stage during growth.

---

* Paper to be given at the International Conference on Lattice Defects in Quenched Metals, Argonne, Illinois, June 15-17, 1964.

INTRODUCTION

The migration of vacancies, and the nucleation and growth of vacancy clusters has been studied in quenched copper by electrical resistivity,[1-5] and small angle scattering of x-rays[4,6,7] and the electron microscope[4-6,8-11] has been used to identify defects formed after precipitation of vacancies.

In a recent paper, Clarebrough et al[5] studied in some detail the effect of various quenching conditions on the isochronal annealing behavior of copper. For samples quenched from a carbon monoxide atmosphere the resistivity decreases in two distinct stages of approximately equal magnitude. 75% of stage I resistivity annealed out in the temperature range -25 to 25°C. This stage was attributed to divacancy annealing by analogy with results for silver. There was very little change in resistance between 100 and 200°C. Stage II occurred between 200 and 400°C and was attributed to the annealing out of submicroscopic vacancy clusters or prismatic loops. A more complicated annealing behavior was observed when specimens were quenched from an argon atmosphere. This complication appears to be due to oxygen contamination.

Analysis of small angle scattering measurements made in quenched copper aged at, or slightly above, room temperature suggest that vacancy clusters have spherical shapes[4] or perhaps are oblate ellipsoids.[7] Clusters were first detected after about 30 minutes aging at 25°C and reached a maximum size of ~30Å after 2 hours.[4]

The first observable defect in copper after quenching is the so-called "black spot". Chik et al[6] found small dark spots (90% with diameter below 80Å) in rapidly quenched copper aged for two hours at 80°C. In

some cases spots could be identified as dislocation loops with double arc contrast. No detailed contrast analyses of the defects was reported. On the other hand, Clarebrough et al[5] found no evidence for any type of point defect clusters in copper quenched from carbon monoxide. Nevertheless, for foils quenched from argon, a high concentration of dislocation loops was always observed. Most of these loops appeared in rows along <110> directions and are characteristic of loops produced by prismatic punching.[11,12] It is generally assumed that the precipitate particles responsible for prismatic punching arise from the oxidation of trace impurities at the quenching temperature. The absence of prismatic punching in specimens quenched from vacuum[11] and carbon monoxide[5] support this argument.

It is quite evident now that impurity atoms[5,13-16] and plastic deformation[17-19] can markedly effect the migration of vacancies and the nucleation of vacancy clusters following quenching. The effect of these two factors can, in part, account for the widely differing results that have been reported for copper, silver, gold and aluminum.[20]

In the present work, copper single crystal were gas quenched from vacuum. Transmission electron microscopy was used to study the subsequent precipitation of vacancies. Single crystals were selected in order to facilitate diffraction contrast analysis and to eliminate the influence of the anisotropy in the coefficient of expansion at or near grain boundaries.[20] Gas quenching from a vacuum was employed in order to prevent contamination from oxygen, to minimize plastic deformation which is usually associated with "drop" quenching, and to obtain easily, reproducible temperature-time characteristics during the quench. The paper

describes some preliminary results; emphasis is placed on the techniques employed.

EXPERIMENTAL PROCEDURE

Single crystals of the desired orientations were grown from 99.999+% copper* in graphite crucibles by a modified Bridgman technique. Crystals were cut by spark erosion, chemically thinned to the appropriate thickness, annealed in the quenching chamber under a dynamic vacuum, and gas quenched in a directed spray of pre-cooled helium. Quenched and aged samples were electropolished for examination in the electron microscope. Throughout all of the above procedures, precautions were taken to avoid contamination and deformation of the samples.

A. Specimen Preparation

Sections of the as-received 1.88 cm dia copper rod were cold rolled to 0.05 cm thick strips without any intermediate annealing. These strips were sheared to size (1.88 cm x 25.4 cm), etched in dilute HNO_3 to remove any surface contamination, rinsed in distilled water and carefully dried. This material was then used as the charge for growing single crystals with <111> and <110> foil normals. The polycrystalline strips were inserted into a previously outgassed, split, graphite crucible (National Carbon Company AUC grade) along with a seed crystal of the desired orientation.

---

* High purity copper, grade A-58 supplied by American Smelting and Refining Company, Central Research Laboratories, South Plains Field, New Jersey. No impurities are detectable by spectrographic analysis. Selenium plus sulfur are less than 1 ppm.

Crystals were grown in a dynamic vacuum of about 2×10^{-6} mm Hg at a rate of 2in. per hour. Induction heating was employed. Seed crystals were prepared in a similar manner from suitably oriented, spherical single crystals. Orientations were determined by the standard Laue back reflection technique and found to lie within a few degrees of the desired orientations.

Single crystals were cut into 1 cm lengths using a "servomet" spark cutter and them chemically thinned to ~0.01 cm thickness in a solution of 50% nitric acid, 25% glacial acetic acid, and 25% phosphoric acid.

B. Annealing, Quenching and Aging Techniques

Following chemical thinning, specimens ~0.01 cm x 1.0 cm x 1.88 cm were placed in a fused quartz support (see Fig. 1-a) which was designed to minimize contact with the foil and to accommodate dimensional changes. Samples were then annealed in the quenching chamber (see Fig. 1-b) under a dynamic vacuum (~2×10^{-6} mm Hg) for one hour at 800°C. Induction heating was employed. The temperature was then slowly raised until local melting (1050-1060°C as shown by thermocouples attached to a specimen) was induced. This usually took about 30 minutes.

The specimens were quenched in a directed spray of purified helium gas which was pre-cooled to -196°C. For this purpose the helium was admitted through a vacuum solenoid valve and the induction power cut to zero simultaneously. The gas passed through two frits* which were 30 mm

* Dow Corning Fritted Glass Ware - extra coarse (170-200μ porosity).

in diameter and separated by a distance of about 2 cm. The flow was directed perpendicular to the foil surface. The specimen assumed a stable position between the two frits.

The change in temperature of the foil during a quench was observed oscillographically and profiles photographed using a Polaroid camera. Platinum-platinum 10% rhodium thermocouple wires (0.025 cm dia) were sintered to polycrystalline copper foils of the same dimensions as the single crystals previously discussed. The thermal emf of the couple was then measured during the quench. It was found that, for a fixed specimen size and pressure of helium in the resevoir, quenching conditions were completely reproducible over the entire temperature range. A temperature-time profile characteristic of the quenching conditions employed in this work is shown in Fig. 2. The average quenching rate for the first 500°C is about 5,000°C/sec. This value is probably an underestimate of the quenching rate of the foil itself because of the nature of the specimen-thermocouple geometry.

A range of aging conditions are presently under investigation. In this preliminary report only the results of aging at room temperature for 15 minutes followed by "up-quenching" to 100°C will be presented. A constant temperature bath of silicon oil (Dow Corning 704 Fluid) was used for the 100°C treatments.

C. Preparation of Electron-Transparent Foils

The specimens were electropolished at room temperature in a 25% H_3PO_4, 25% ethyl alcohol, and 50% distilled water electrolyte to thickness just

slightly greater than that necessary for good transmission of electrons. Final thinning was done in a 33% nitric acid and 67% methyl alcohol solution maintained at about -60°C. In all cases a special specimen mount was used so as not to deform the foil during thinning.

D. Techniques for Identifying Observed Defects

A Siemens Elmiskop I electron microscope, operated at 100 kV and equipped with a double tilting stage device,[21] was used for observation of the specimen. With this stage the specimen is mounted in such a way that no deformation occurs. All dark field images were obtained by tilting the electron gun until the desired diffracted beam passed down the center of the microscope column. The reasons for taking dark field images will subsequently be discussed, but first, it is important to point out the geometric changes accompanying gun tilting.

Referring to Fig. 3, normal operation of the microscope is as shown in part (a); the incident electron beam makes an angle θ, the Bragg angle, with a set of diffracting planes in the crystal. The transmitted and diffracted beams intersect the Ewald sphere at reciprocal lattice points separated by a characteristic reciprocal lattice vactor, $\vec{g}$. In the case of electron waves the reflecting sphere is almost plane and coincides with the back-focal-plane of the objective lens of the microscope. Bright field images are obtained by placing an aperture in the center of the microscope column which allows only the transmitted beam to be observed and diffraction contrast results from the elimination of scattered beams. The aperture can be moved to allow passage of only

the diffracted beam, thus obtaining a dark field image but images obtained in this manner are usually unsuitable for any quantitative work because of the spherical aberration of the magnetic lenses in any off-centered beam. To eliminate this defect and to obtain higher resolution the electron gun is tilted so as to allow the diffracted beam to pass down the center of the microscope column as shown in Fig. 3-b. When one wishes to observe a particular field of view that exists for a strong two-beam case in bright field, the electron gun is tilted away from the operating reflection through an angle equal to twice the Bragg angle for the particular set of diffracting planes giving strong diffraction: this angle is of the order of a few degrees for electron waves. The result is that the diffracting planes for dark field are the negative of those used in bright field and the diffracted beam passes down the center of the microscope column without being subjected to aberration by the lenses. Thus the operating reflection for a gun-tilted dark field is the negative of the operating reflection for a bright field image. Two beam cases are easily achieved with the double-tilt specimen holder.

For observation of defects which are too small to be resolved with the electron microscope, one must resort to methods other than imaging the defect itself by diffraction contrast. In the case of small inclusions in the matrix which cause local straining of the lattice, the presence of such defects can be detected by strain contrast although the actual defect cannot be observed. The theory of strain contrast from inclusions has been presented in two papers by Ashby and Brown.[22,23] Within half an extinction distance of either surface, at or near ideal Bragg conditions (s=0), the image caused by the strain field of the defect is one which

consists of dark and white areas, semi-elliptical in appearance, separated by a line of no contrast perpendicular to the strain vector of the defect (see Fig. 4). In bright field the black-white image of a defect near the bottom of the foil will be the reverse of the black-white image of an identical, and similarly oriented defect near the top surface of the foil. However, in dark field, black-white images of defects are the same near the top and bottom surfaces, and in dark field the normal to the line of no contrast and the direction of the operating reflection, $\bar{g}$, make (a) an acute angle on the white side of the black-white image for vacancy-type inclusions, and (b) an acute angle of the black-side of the black-white image for interstitial-type inclusions.(23)

Thus, in order to identify unambiguously the character of the defect, whether vacancy or interstitial, it is necessary to use dark field techniques to distinguish between the two cases, since for a given defect it is not possible to tell whether it is near the top or the bottom surface with only a bright field image.

Furthermore, before comparing the images with the diffraction pattern to determine how the operating reflection lies with respect to the line of no contrast, all rotations and inversions of the micrograph with respect to the diffraction pattern must be accounted for.

The Burger's vector of the defect can be analyzed from the dark field image by observing the direction of the normal to the line of no contrast and comparing that normal with the projections of possible Burger's vectors onto the surface of the foil, e.g., a Frank loop showing strain contrast will exhibit a line of no contrast perpendicular to a <111> direction lying in or projected onto the plane of the foil. This technique was used by

Essmann and Wilkins[24] to determine that the black-dot defects formed by neutron irradiation of copper were primarily Frank sessile vacancy loops.

It is important to distinguish between the line of no contrast of the image and the so-called quasi-symmetry line pointing from black-to-white. These lines may or may not be perpendicular depending on the orientation of the defect. In Fig. 4-a there are three distinguishable black-white directions, but there are four zero-contrast lines. These cases are illustrated in Fig. 4-b. Cases A, C, and D have zero-contrast lines perpendicular to their black-white directions, but case B has a zero-contrast line which lies normal to the direction of a projected <110> vector whereas its black-white direction is along a <111> direction in the plane of the foil. Thus, the zero-contrast line and the black-white direction are normal when the Burger's vector lies in the plane of the foil, such as in cases A and D, or when the Burger's vector of the defect lies normal to the defect plane, such as in case C. The two lines will not be normal in those cases where the Burger's vector of the defect is not in the plane of the foil and does not lie perpendicular to the defect plane, such as in case B.

RESULTS

Since the white side of the strain contrast image in almost all cases lies to the same side of the zero-contrast line as does the operating reflection vector, $\bar{g}$, for all foil orientations and all operating reflections, the defects produced in our experiments are all due to vacancies.

The fact that the line of no contrast of the image makes various angles with the operating reflection vectors (they are perpendicular only for <220> and <111> reflections otherwise the zero-contrast line lies perpendicular to <110> and <111> directions projected onto the plane of the foil), indicates that the vacancy-type defects are planar rather than spherical, since straining of the crystal only takes place in certain crystallographic directions. A spherical defect would always exhibit a zero-contrast line perpendicular to the operating reflection vector regardless of which vector it was.

The fact that the lines of no contrast are in some cases perpendicular to distinct <111> directions and in other cases perpendicular to distinct <110> directions indicates that the Burger's vectors of the defects are of two types, $\frac{a}{2}$ <110> and $\frac{a}{3}$ <111>, and thus unreasolvable prismatic loops, both perfect and imperfect are present.

The perfect prismatic vacancy loops, with Burger's vectors of the type $\frac{a}{2}$ <110>, appear to be the more numerous and in general the larger, ranging in size from 100Å to about 200Å. The imperfect prismatic vacancy loops, with Burger's vectors of the type $\frac{a}{3}$ <111>, appear to be slightly less numerous and range in size from perhaps less than 60Å to about 125Å at the largest.

Densities of the defects were obtained by counting the number of defects appearing on micrographs for various areas and using thicknesses equal to single extinction distances (since the defects only show strain contrast within half an extinction distance of either surface) and taking the ratio of the number of defects to the enclosing volumes. Multiplicity factors of 6 for $\frac{a}{2}$ <110> type defects and of 4 for $\frac{a}{3}$ <111> type defects

were used to account for defects on other systems not in positions to give rise to strain contrast, assuming homogeneous nucleation. The density of perfect loops was calculated to be about $4 \times 10^{15}/cm^3$ and that of the imperfect loops about $3.5 \times 10^{15}/cm^3$. Thus the maximum defect concentration is about $7.5 \times 10^{15}/cm^3$. Assuming an average loop diameter of 125Å and a vacancy concentration related to the defect concentration by $C = \pi r^2 bN$, it is concluded that the quenched in vacancy concentration must be at least 2×10^{-5} in order to account for the estimated loop density.

The type of defect observed depends to a great extent upon the operating reflection for contrast. For some beams operating, an area might appear almost completely devoid of defects as shown in Fig. 5-a, whereas, another beam operating in the same field of view will give rise to strain contrast and disclose the presence of defects as shown in Fig. 5-b. If a <220> reflection is used the primary defect observed will be one whose Burger's vector lies along the operating reflection as in Fig. 6, that is, an $\frac{a}{2}$ <110> type. If a <111> reflection is used, as in Fig. 7, the defect most likely to be observed will have a Burger's vector of type $\frac{a}{3}$ <111> lying along the direction of the operating reflection. If a reflection such as <200> in a [110] foil is used, then two $\frac{a}{3}$ <111> systems are resolved as shown in Fig. 8 and no $\frac{a}{2}$ <110> systems. Lastly, if an operating reflection is used which lies between a <111> and a <220> direction in the plane of the foil, both systems will be imaged as already demonstrated in Fig. 4. In any case, the most easily observed defects will have Burger's vectors which lie in the plane of the foil. Defects with Burger's vectors not in the plane of the foil will give rise to weaker strain

contrast and may be entirely invisible if the angle between the Burger's vector and the plane of the foil is large.

Finally it should be noted that on one occasion defects were observed which appear to be interstitial loops (Fig. 7). Presumably, these arise from some mechanism associated with impurities. However, no punched defects of the type reported elsewhere[11,12] have been observed in our work.

DISCUSSION

The results show that, when copper single crystals are quenched from vacuum under the conditions stated and subsequently aged for 15 minutes at room temperature and then 1 hour at 100°C, randomly oriented, planar, vacancy aggregates are produced. Both perfect and imperfect prismatic loops occur, but the former appear to be more numerous. The maximum size of Frank loops does not exceed 125Å, whereas, perfect loops range in size from 100 to 200 Å.

These observations, together with previous results obtained from small angle x-ray scattering experiments[4,7] suggest that the precipitation of vacancies follows the sequence, vacancy clusters → imperfect prismatic loops → perfect prismatic loops. It is of interest to estimate which type of defect is to be expected on the basis of the dislocation line energy and the stacking fault energy.

The relative energies of a stacking fault tetrahedron, a stacking fault loop, and a perfect prismatic loop that could form from a given number of vacancies can be estimated if a value of the stacking fault

energy for copper is assumed. They are given approximately by:[20]

$$E_T = \frac{Ga^2\ell}{12\pi(1-\nu)} \ln\left(\frac{\ell}{r_o}\right) + \sqrt{3}\,\ell^2\,\gamma$$

$$E_L = \frac{Ga^2\ell}{4\pi(1-\nu)} \ln\left(\frac{\ell}{r_o}\right) + \frac{\sqrt{3}}{4}\ell^2\,\gamma$$

$$E_P = \frac{Ga^2\ell}{2\cdot 4(1-\nu)} \ln\left(\frac{2\ell\sqrt{2}}{a}\right),$$

where E_T, E_L, and E_P are the energies of a tetrahedron, a triangular stacking fault loop and a triangular perfect loop respectively, each having side ℓ. G is the shear modulus, a the unit cell dimension, r the dislocation core radius, ν is Poisson's ratio, and γ is the stacking fault energy.

These energies are shown as a function of ℓ in Fig. 9 taking γ = 70 ergs/cm^2.[25] The activation energy required to convert one type of defect to another has been neglected. The results obtained are quite sensitive to the selected value of γ.

On the basis of these calculations the tetrahedron appears to be the stable defect in the range of ℓ which is experimentally observed. However, no tetrahedra have been resolved in the present work. In order to account for this discrepency one would have to assume that the nucleation of such a defect in copper is difficult. Assuming this to be the case, then the triangular stacking fault loop has the lowest energy below a critical size (ℓ_o ~200Å for γ = 70 ergs/cm^2). The present results are in qualitative agreement with the existence of such a critical size.

Whilst small tetrahedra have not yet been observed in quenched copper, it is possible that the initial vacancy clusters may have tetrahedral shapes.

The form of the initial precipitate will depend upon the supersaturation of vacancies and nucleating conditions. Additional work is now being done in an attempt to identify the nature of the initial defect. This requires detailed examination of quenched and low-temperature aged specimens.

ACKNOWLEDGEMENTS

We wish to thank the auspices of the United States Atomic Energy Commission for continued financial support of our research program through the Inorganic Materials Research Division of the Lawrence Radiation Laboratory, University of California, Berkeley.

REFERENCES

1. G. Airoldi, G. L. Bachella, and E. Germagnoli, Phys. Rev. Letters 2, 145 (1959).
2. W. Schüle, A. Seeger, F. Ramsteiner, D. Schumacher, and C. E. Ransley, Z. Naturforsch 16a, 323 (1961).
3. D. G. Martin, Phil. Mag. 7, 803 (1962).
4. J. Galligan and J. Washburn, Phil. Mag. 8, 1455 (1963). See also Lawrence Radiation Laboratory Report UCRL 10606.
5. L. M. Clarebrough, R. L. Segall, M. H. Loretto, and M. E. Hargreaves, Phil. Mag. 9, 377 (1964).
6. K. Chik, A. Seeger, and M. Ruhle, Proceedings of the 5th International Congress on Electron Microscopy (Academic Press Inc., New York, 1962), p. J-11.
7. A. Seeger, V. Gerold, and M. Ruhle, Zeitschrift für Metallkunde 54, 493 (1963).
8. R. E. Smallman, K. H. Westmacott, J. H. Coiley, J. Inst. Metals 88, 127 (1959).
9. R. E. Smallman, K. H. Westmacott, J. Appl. Phys. 30, 603 (1959).
10. P. B. Hirsch and J. Silcox, Growth and Perfection of Crystals (John Wiley & Sons, Inc., New York, 1958), p. 262.
11. R. S. Barnes and D. J. Mazey, Acta Met. 11, 281 (1963).
12. A. Eikum and G. Thomas, Acta Met. 12, 537 (1964).
13. R. M. J. Cotterill and R. L. Segall, Phil. Mag. 8, 1105 (1963).

14. L. J. Cuddy and E. S. Machlin, Phil. Mag. 7, 745 (1962).

15. D. Jeannotte and E. S. Machlin, Phil. Mag. 8, 1835 (1963).

16. R. L. Segall and L. M. Clarebrough, Phil. Mag. 9, 865 (1964).

17. J. Takamura, Acta Met. 9, 547 (1961).

18. J. J. Jackson, Acta Met. 11, 1245 (1963).

19. G. Das and J. Washburn, Lawrence Radiation Laboratory Report UCRL-11188.

20. G. Thomas and J. Washburn, Rev. Modern Phys. 35, 992 (1963).

21. G. V. Patser and P. R. Swann, J. Sci. Instr. 39, 58 (1962).

22. M. F. Ashby and L. M. Brown, Phil. Mag. 8, 1083 (1963).

23. M. F. Ashby and L. M. Brown, Phil. Mag. 8, 1649 (1963).

24. U. Essmann and M. Wilkens, Phys. Stat. Sol. 4, K53 (1964).

25. P. R. Thornton, T. E. Mitchell and P. B. Hirsch, Phil. Mag. 7, 1349 (1962).

Figure Captions

Fig. 1. Quenching apparatus.

(a) Specimen holder.

(b) Quenching chamber.

Fig. 2. Change in temperature as a function of time corresponding to a helium, reservoir pressure of 20 psi.

Fig. 3. Imaging conditions for bright and dark field operation.

(a) Normal bright field conditions.

(b) Dark field conditions after gun-tilting.

Fig. 4. (a) Dark-field micrograph showing strain contrast from vacancy precipitates.

(b) Sketch of the four identifiable defect systems.

Fig. 5. (a) Dark-field micrograph of region showing only a very small amount of strain contrast with operating reflection $\bar{g} = [\bar{3}11]$.

(b) Dark-field of same area using the $[02\bar{2}]$ reflection. Inclusions with Burgers vectors parallel to the operating reflection show strain contrast. Foil normal is [233] (about 10° from [111]).

Fig. 6. Dark-field micrograph showing strain contrast when a <220> beam is used. The primary defects appearing are perfect vacancy loops having the Burger's vectors parallel to the operating reflection.

Fig. 7. Dark-field micrograph showing strain contrast observed when a <111> beam is used. The primary defects observed are imperfect vacancy loops with Burger's vector parallel to the operating reflection. Notice the $\frac{a}{2}$ <110> loops appearing at F and the inclusions at G exhibiting strain contrast that would be expected from an interstitial type inclusion. Foil normal is [110].

Fig. 8. Dark-field micrograph showing strain contrast appearing when the $[00\bar{2}]$ beam is used in a [110] foil. Weak strain contrast is exhibited by two systems of imperfect defects H and J lying on the two <111> plane normal to the plane of the foil.

Fig. 9. Defect energies for copper as a function of size.

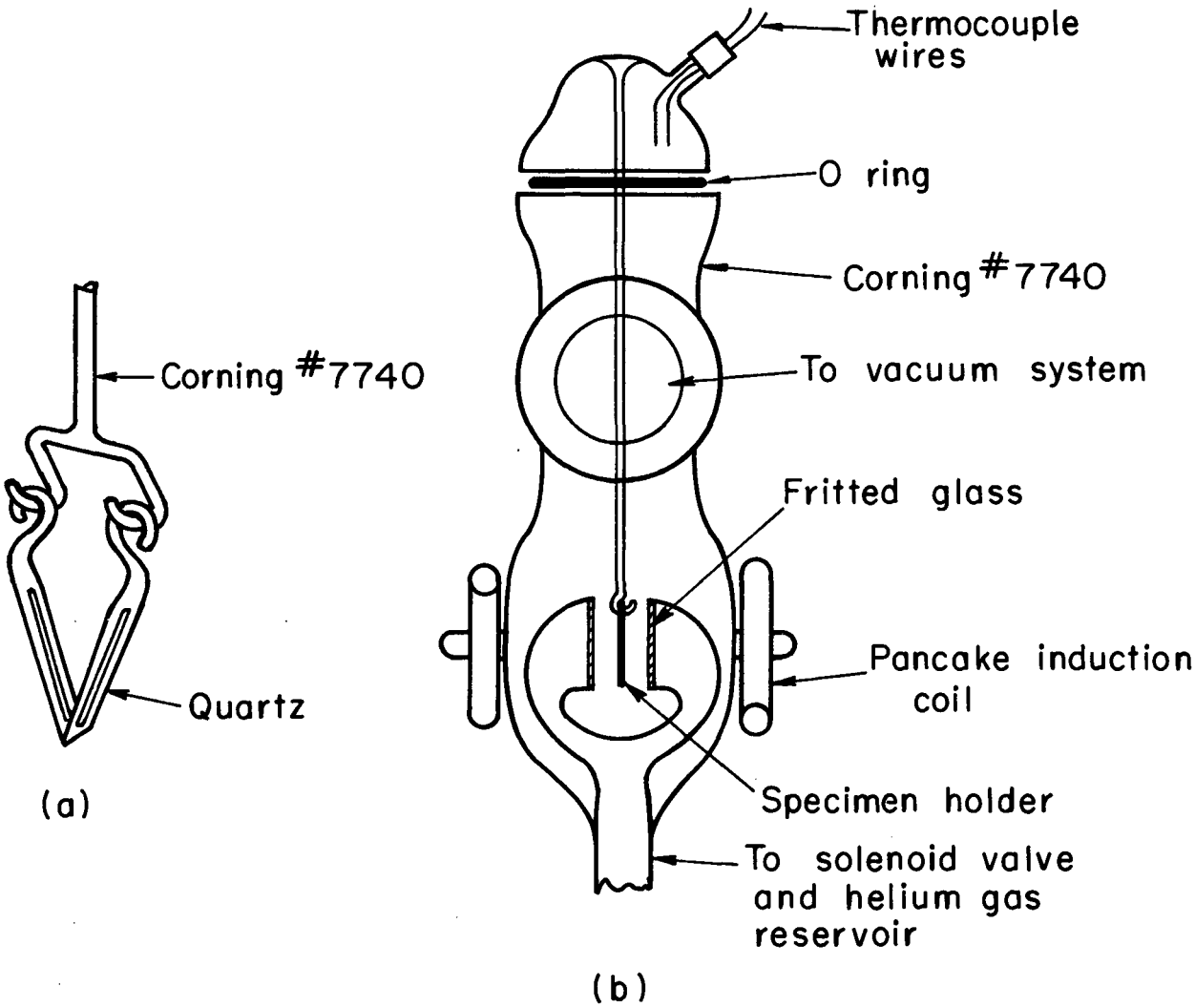

MUB-3767

Fig. 1

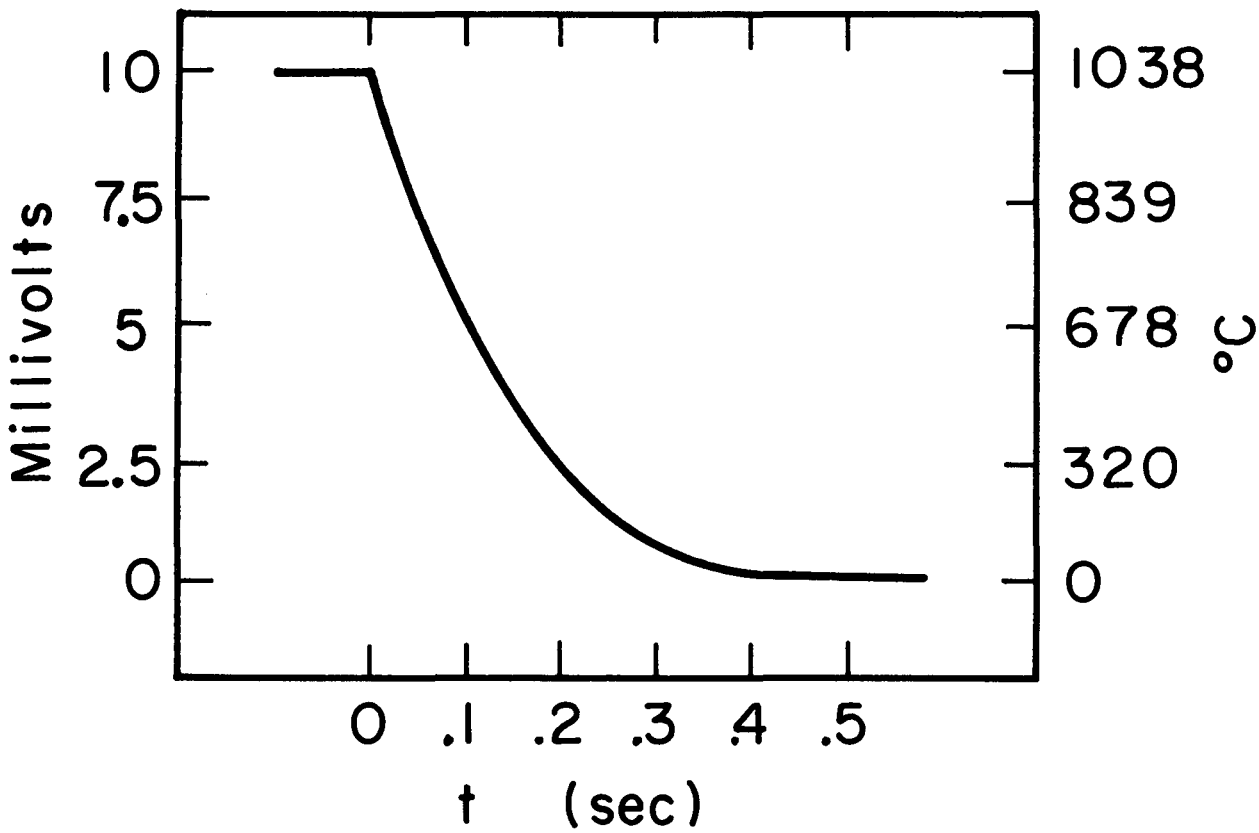

MUB-3764

Fig. 2

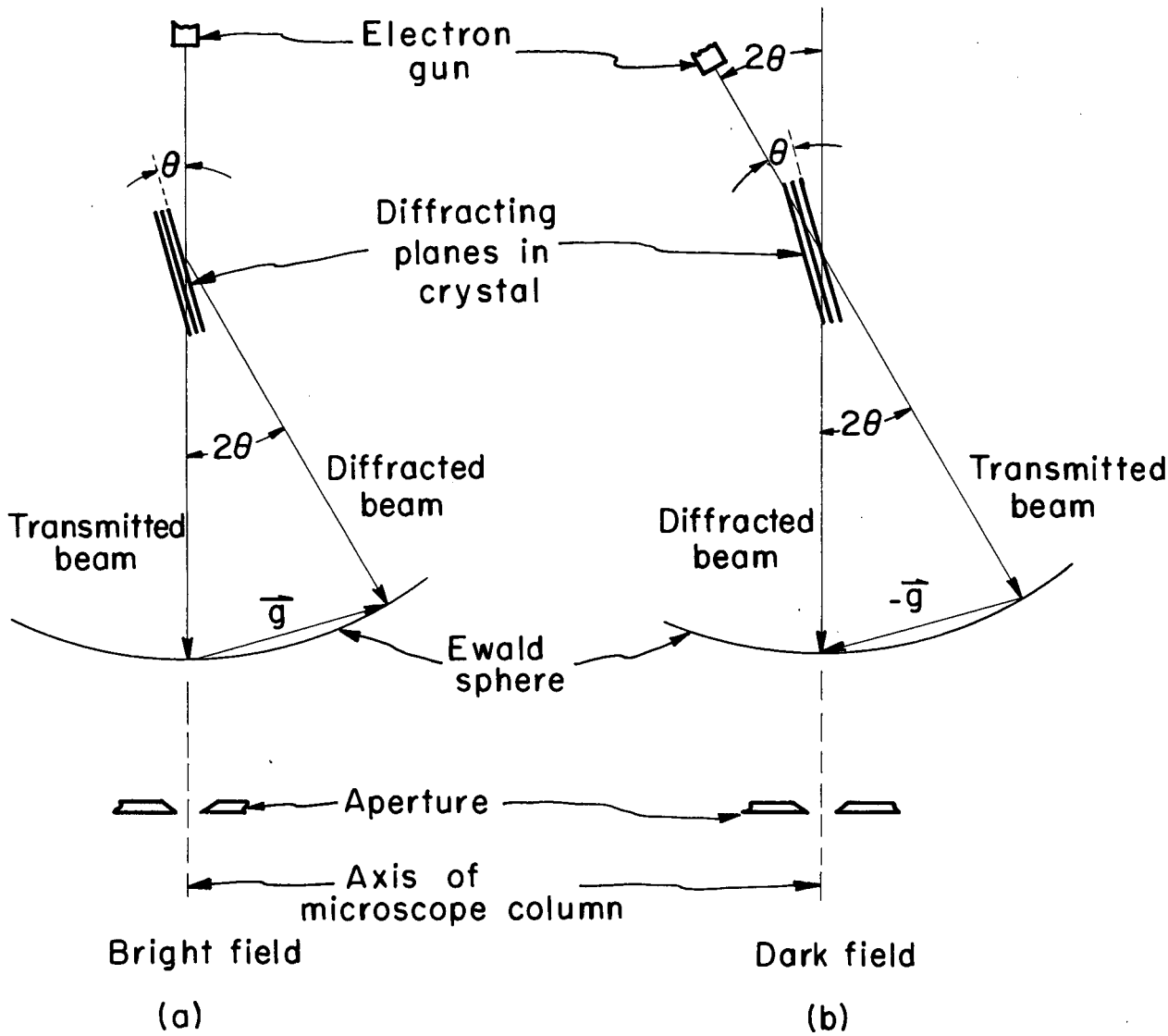

MUB-3766

Fig. 3

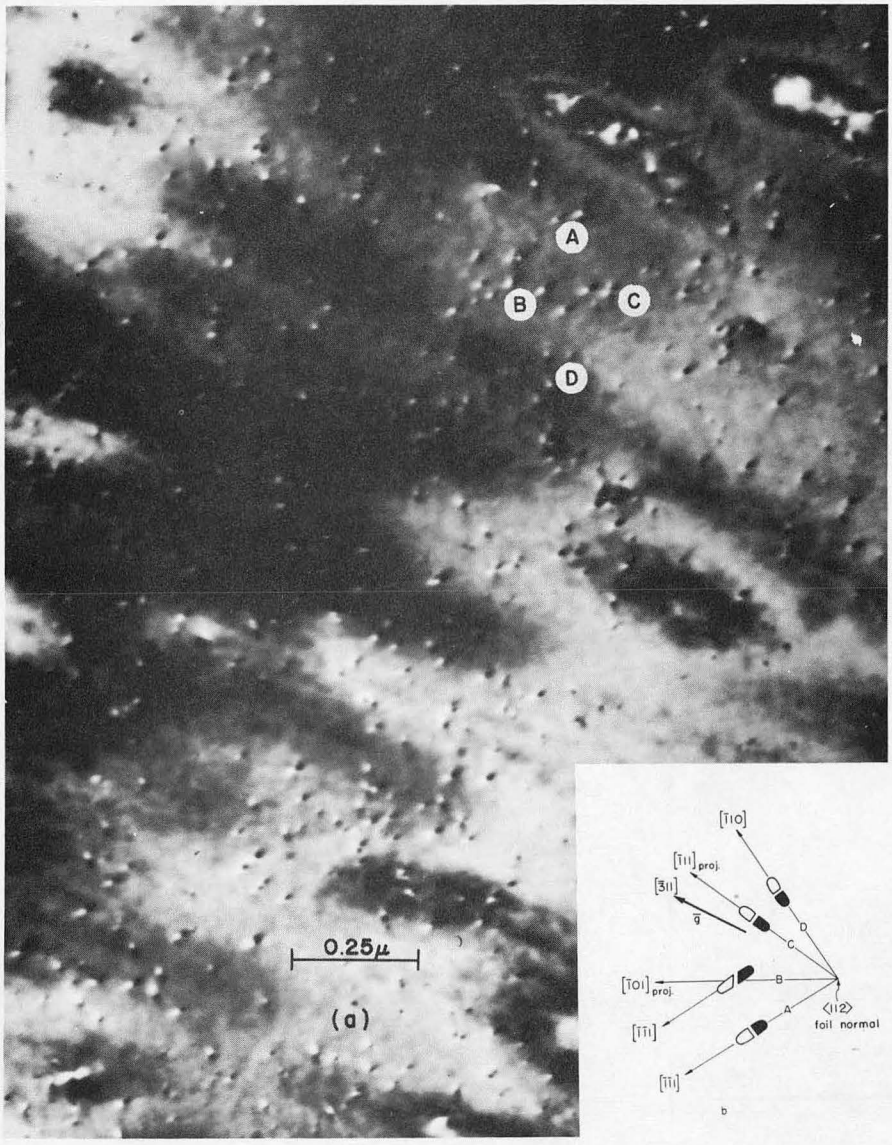
A
B
C
D
0.25μ
(a)
[1̄10]
[1̄11]proj.
[3̄11]
g
D
C
[1̄01]proj.
B
A
⟨112⟩
foil normal
[1̄1̄1]
[1̄11]
b

ZN-4388

Fig. 4

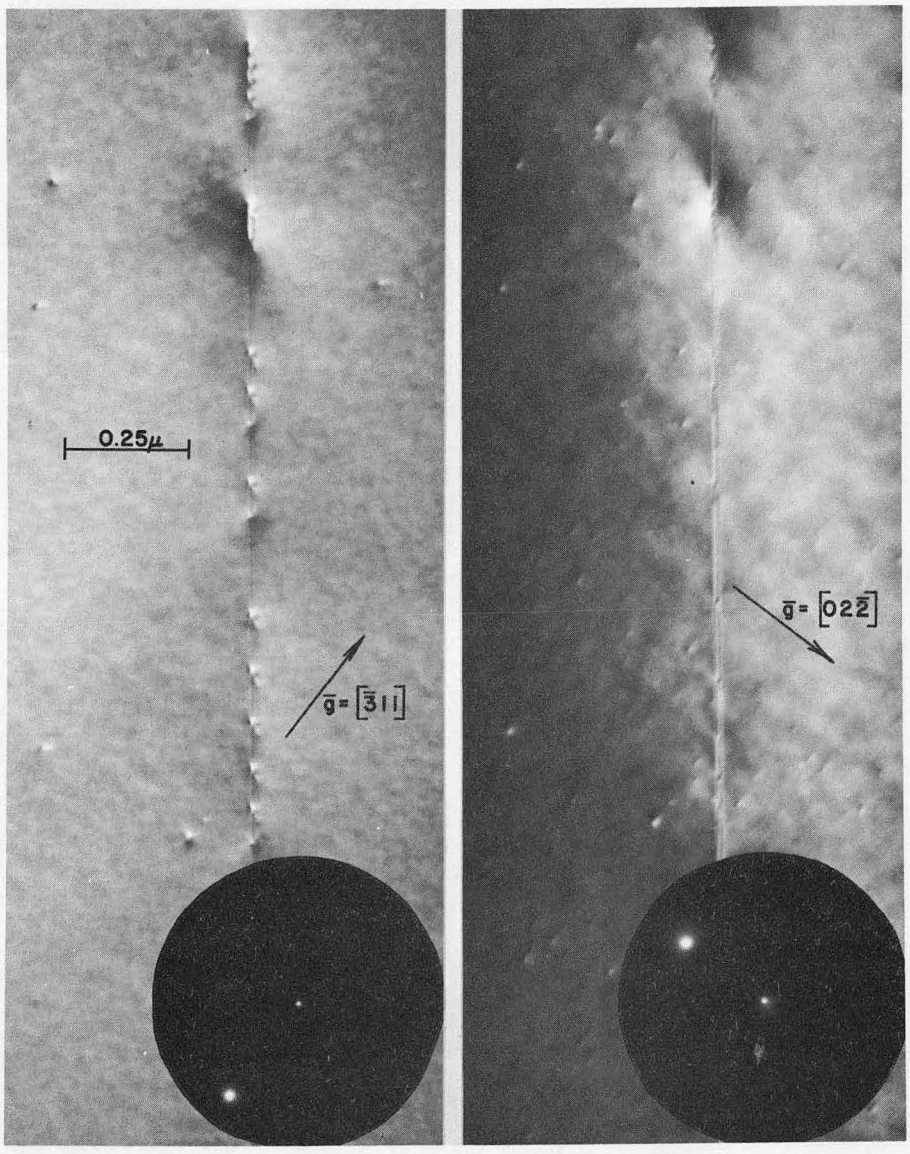

ZN-4389

Fig. 5

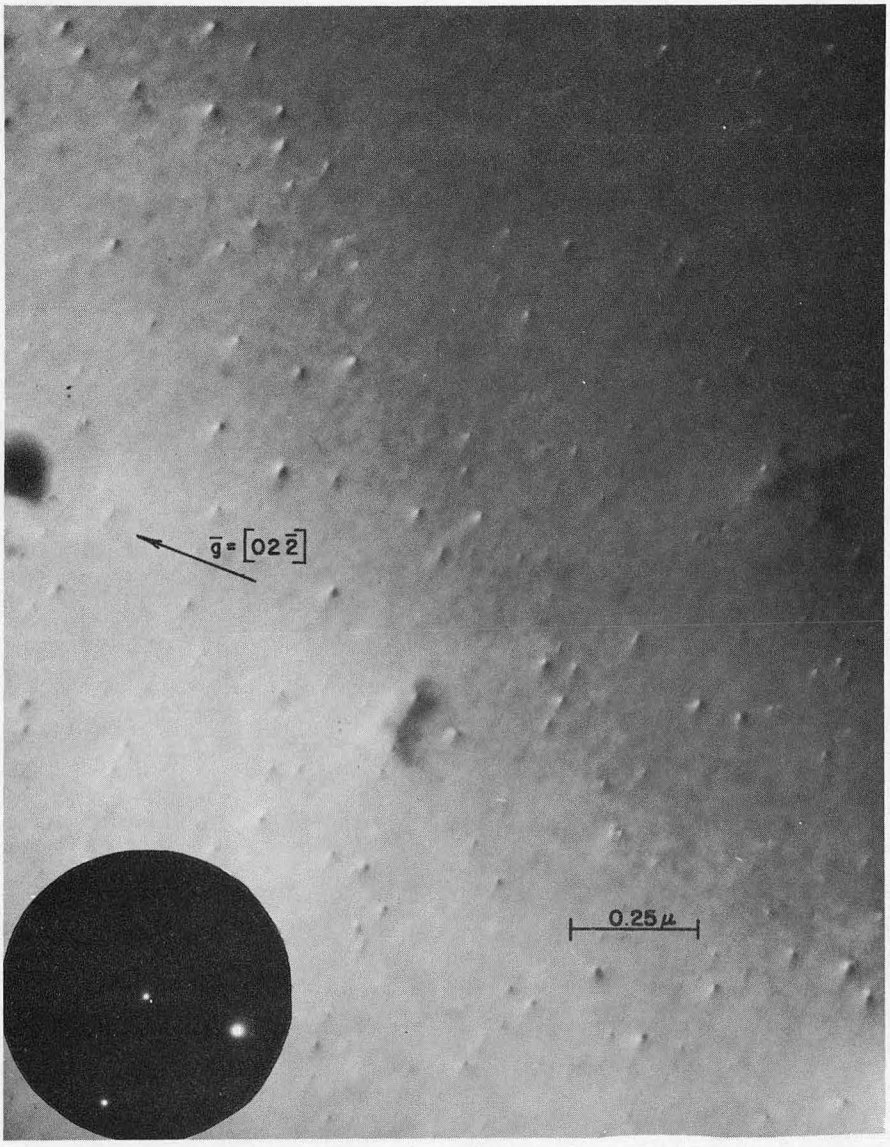

ZN-4390

Fig. 6

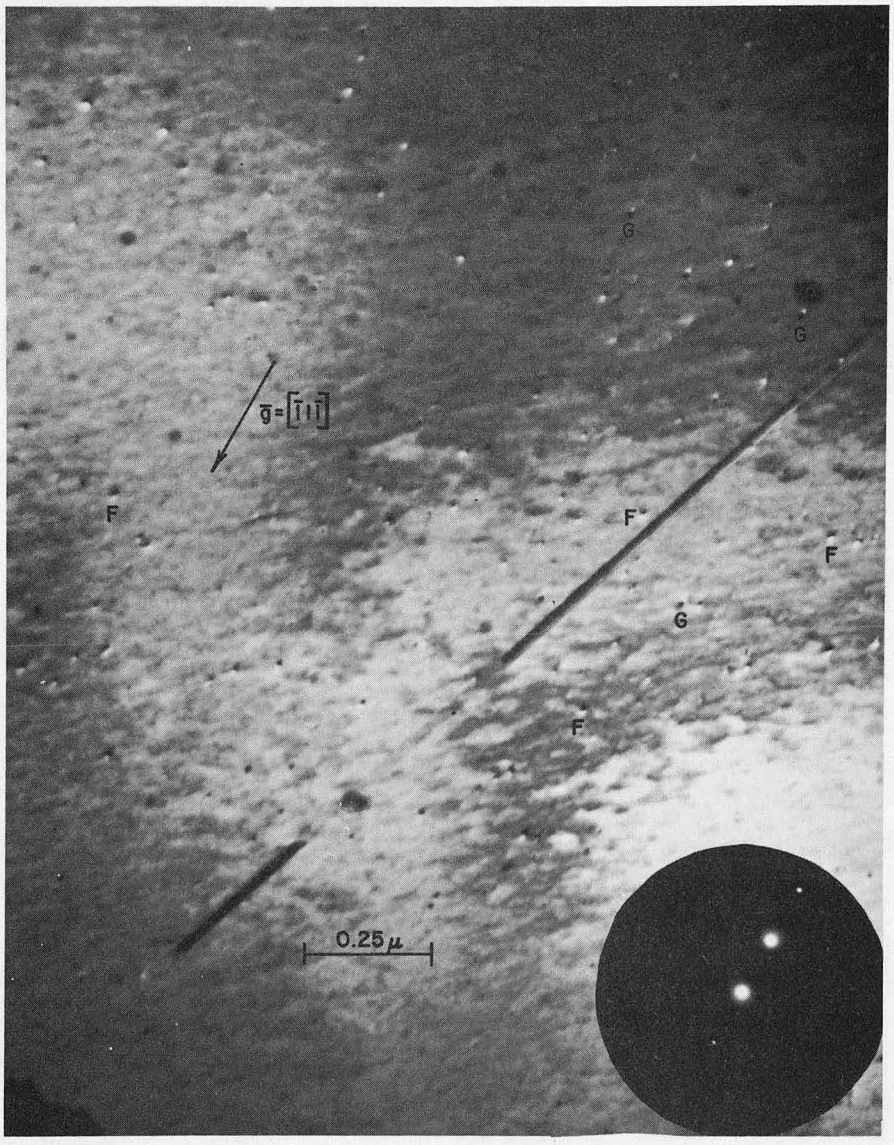

ZN-4391

Fig. 7

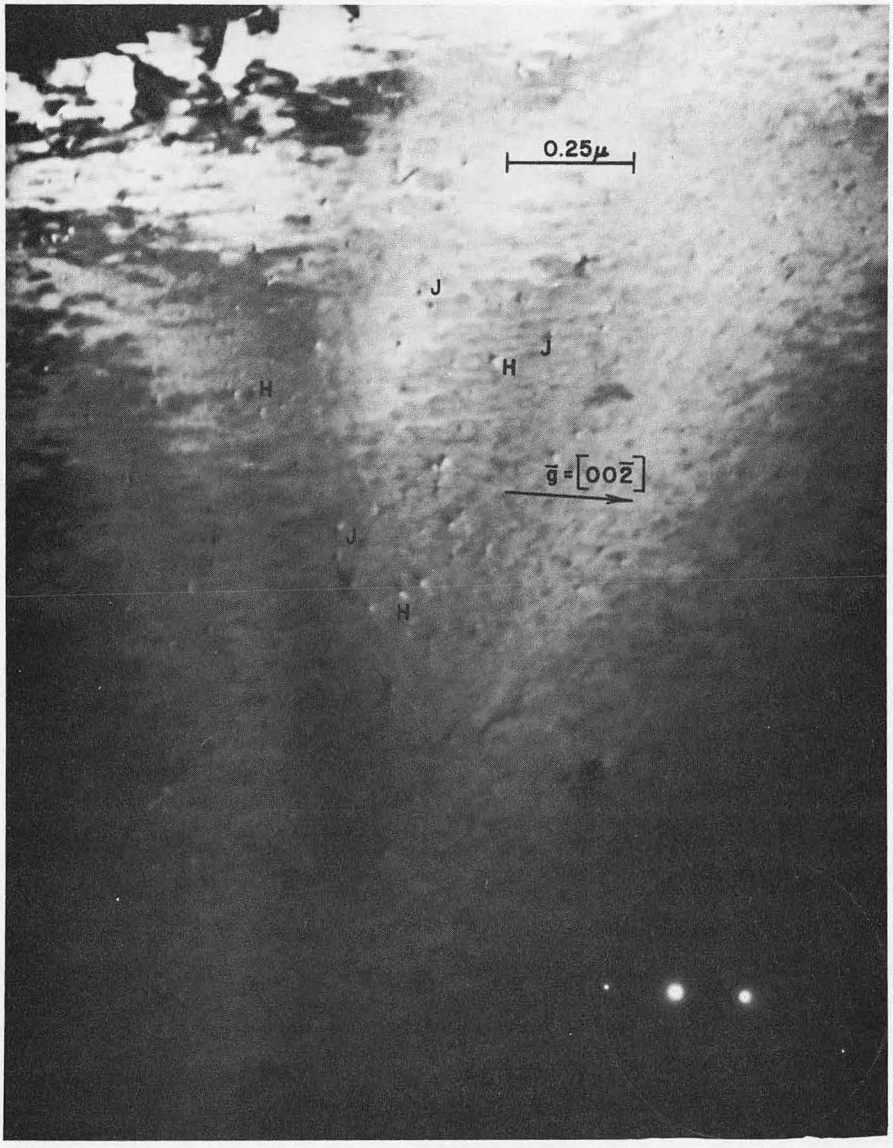

ZN-4392

Fig. 8

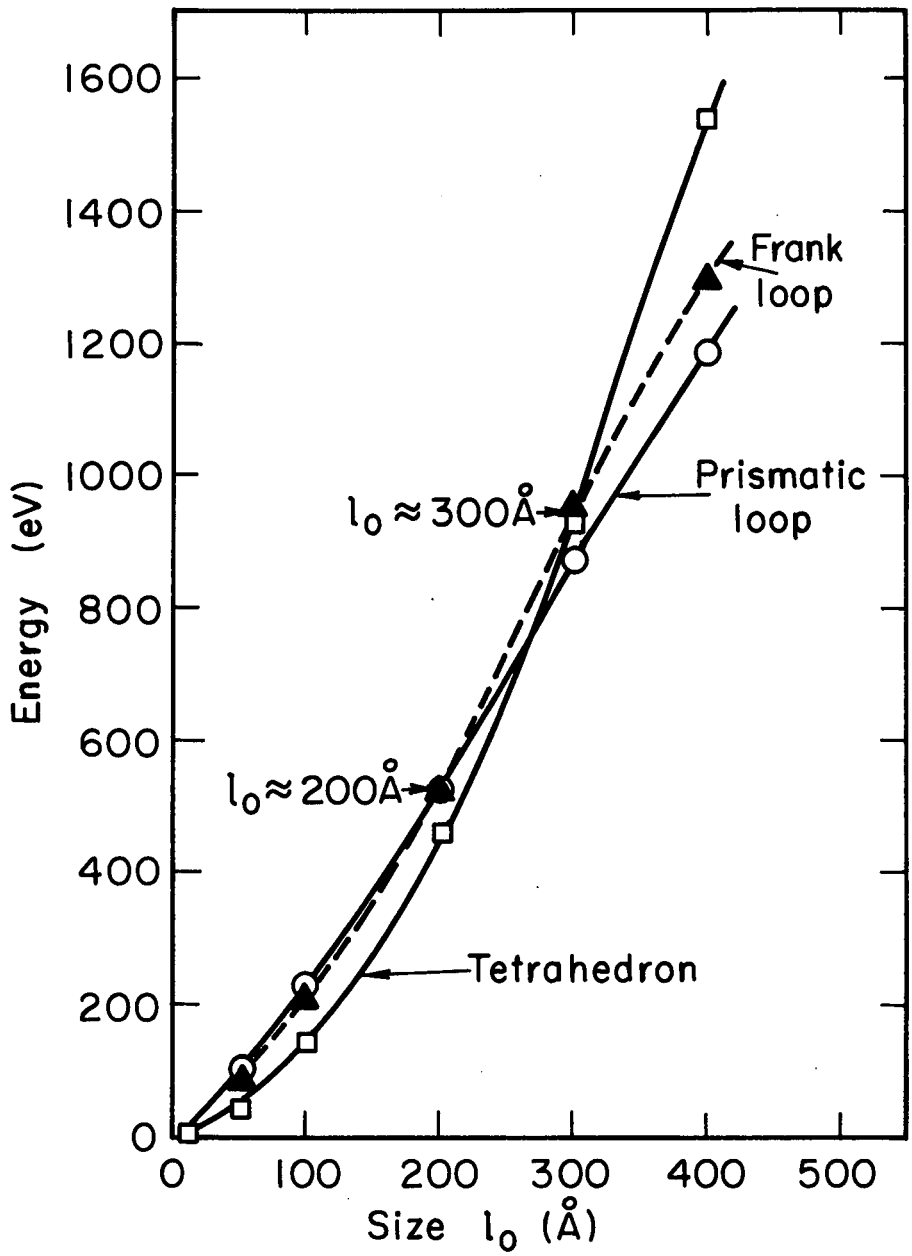
1600
1400
1200
1000
800
600
400
200
0
Energy (eV)
0
100
200
300
400
500
Size l_0 (Å)
Frank loop
Prismatic loop
$l_0 \approx 300$Å
$l_0 \approx 200$Å
Tetrahedron
MUB-3765

Fig. 9

AUTHORS' REPLIES TO DISCUSSION

The two main questions raised in regard to our work concerns the possibility of damage in the microscope and the observed contrast effects. The latter point has already been discussed in some detail in the paper. We wish to dispel all doubt that what has been observed is the result of ion damage in the microscope for the following reasons:

(1) The size and density of defects observed is independent of the time of viewing in the microscope. Some perfect loops occasionally glide out of the foil after prolonged exposure. As pointed out by Cotterill this fact alone proves that the defects are not produced in the microscope.

(2) These defects are not observed in annealed Cu foils.

(3) It should be noted that during ion bombardment experiments, conducted in the microscope on copper, by Howe et al., (Appl. Phys. Letters, 3, 125, 1963), spots and loop-like features were produced only when a coated filament was employed. No further damage was reported when so-called "normal operation" was resumed.

Concerning the contrast, we agree with Whelan and, as clearly shown in our paper, for dislocation loops the line of no contrast does not necessarily have to be normal to $\vec{g}$ except when $\vec{g}$ lies parallel to $\vec{b}$ or its projection. The Ashby-Brown strain contrast theory (references 22 and 23) predicts a line of no contrast normal to the Burgers vector of the defect. For very small prismatic loops in copper we found in all cases that this line was normal to either <110> or <111> directions. The theory does not account for the shape of the image, i.e., the direction of "streaking" of the black-white image, when the strain vector of the defect is not normal to the defect plane.

We have been considering this problem in more detail, since the contrast effects can be very useful in analyzing the types of defects. In order to resolve the numerous possibilities, many single crystal orientations must be viewed. Recent results show that for perfect loops ($\vec{b} = \frac{a}{2}\langle 110\rangle$) the line of no contrast and the black to white "streak" are not normal when the Burgers vector of the loop lies in the plane of the foil if the habit plane of the loop is normal to the foil surface. This statement is demonstrated by the accompanied figure which shows the strain contrast images obtained using a $[2\bar{2}0]$ reflection from a foil whose normal is [110] (the same quenching, aging, preparation, and dark field technique have been used). Five defects systems are observed and we refer now to the direction of the black to white "streak". Two, A and E, are streaked in $\langle 111\rangle$ directions with $\frac{a}{3}\langle 111\rangle$ Burgers vectors, two, B and D, are streaked in $\langle 111\rangle$ directions with $\frac{a}{2}[1\bar{1}0]$ Burgers vectors whilst one, C, is streaked in the $[2\bar{2}0]$ direction with the same Burgers vector of $\frac{a}{2}[1\bar{1}0]$. It appears that if both the Burgers vector of a perfect loop and the normal to the defect plane lie in the plane of the foil the direction of streaking (the black-to-white line) lies along the normal to the defect plane in most, but not all, instances. This observed, unusual black-white streaking in the $[1\bar{1}0]$ direction may arise: (a) as a size dependent effect, (b) from being too close to the foil surface which is currently referred to as causing "anomalous images" (and we agree with Meakin that in this sense we are not observing anomalous images in most cases), (c) because the perfect loop, after rotational glide on its prismatic cylinder may lie on some plane close to $(1\bar{1}0)$. Case (a) is doubtful since defects of comparable size show streaking in both $\langle 111\rangle$ and $\langle 110\rangle$ directions and many large perfect loops

in aluminum show streaking in directions not normal to the zero-contrast line.

For a Frank loop the situation is physically identical to the case of GP zones in Al-Cu discussed in Ashby and Brown's second paper in that the strain vector is perpendicular to the habit plane. Here again the line of no contrast is only perpendicular to $\vec{g}$ for cases where $\vec{g}$ and $\vec{b}$ (or its projection) are parallel. The strain contrast image in this case is expected to be symmetrical about both lines (discussed above), as has been observed.

The extinction distance quoted by Whelan is for {111} and we have been using extinction distances up to 600Å, i.e., {311}, so that examination of appreciable thicknesses over which the dark field contrast is of interest (half-extinction distances), is possible for high order reflections.

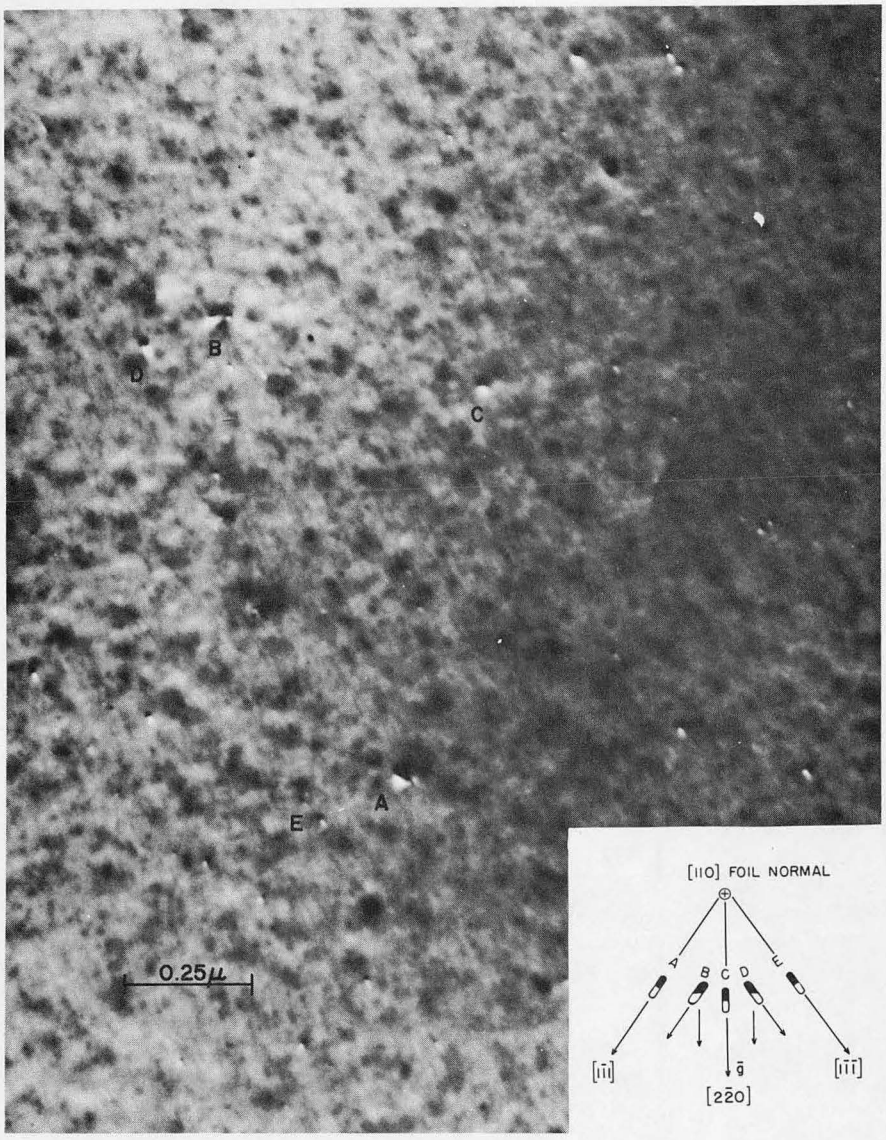

ZN-4393